DOI: 10.13009/EUCASS2023-385
Aerospace Europe Conference 2023 – 10TH EUCASS – 9TH CEAS

Simulation of plume impingement on flat plates via the Fokker-Planck approach

Leo Basov[⋆†] *and Martin Grabe*[⋆]
[⋆]*German Aerospace Center (DLR)*
Bunsenstrasse 10, 37073 Goettingen, Germany
leo.basov@dlr.de · martin.grabe@dlr.de
[†]Corresponding author

Abstract

Simulations of plume impingement on a flat plate using molecular nitrogen were performed by employing the Fokker-Planck (FP) and Direct Simulation Monte Carlo (DSMC) methods. The FP results are in very good agreement with numerical results achieved using the DSMC method while providing a 4 fold speed up when applying the same spatial and temporal resolution. The numerical results were also compared to experimental data measured at the German Aerospace Center (DLR) Goettingen. Both the FP as well as DSMC methods show good agreement with experimental data and reproduce behavior found in literature.

1. Introduction

During their operation in orbit spacecraft make use of rocket thrusters to perform various tasks. A thruster plume can reach and impinge neighboring surfaces due to its spread in high vacuum. This can produce undesired forces or heat loads on especially large areas like solar arrays. Additionally plume impingement can negatively impacting sensitive surfaces like optical diagnostics.[3] Degradation of critical surfaces as well as correction burns which use up valuable propellant can greatly reduce the spacecraft‘s life time. Reliable and accurate modeling of plume impingement effects is therefore an important factor in the design process of spacecraft.[10,14] Leading to impingement the flow exiting a nozzle goes through a wide range of Knudsen numbers as it expands into vacuum and compresses again due to interactions with the surface.[3] These effects can be described by the Boltzmann equation. A common approach to numerically solve it is the Direct Simulation Monte-Carlo (DSMC) method pioneered by Bird.[1] The method is very efficient for high Knudsen numbers but becomes increasingly computationally intensive when approaching the continuum limit. In this flow regime computational fluid dynamics (CFD) methods are normally used as they provide a high level of maturity and efficiency. As problems like plume impingement require the simulation of a wide range of Knudsen numbers a coupled approach using DSMC and CFD methods can be employed. However, this leads to many issues stemming among others from noise produced by DSMC especially at low Mach numbers.[19] Another way to model the flow in the continuum limit is the recently proposed kinetic Fokker-Planck (FP) method[12] which, like DSMC, relies on simulated particles to transport mass, momentum and energy through the flow domain, but does not resolve individual collisions which leads to the comupational time being independent from the Knudsen number. Both DSMC and FP use particles for the discretization of the velocity distribution function. When applying a coherent position integration scheme in the push step, the models can be coupled leading to an efficient simulation method which solves many of the issues one faces when coupling DSMC to classical CFD methods.[8]

Even though the validity of the FP method has only been mathematically shown for very low to moderate Kn numbers,[2] it has been observed that the model can be applied to rarefied gas flows with thermal non-equilibrium with adequate results[5,7] especially when further modifications are considered.[9] This means that FP potentially provides a method to cover a wide application range using a single model.

In this work we investigate how numerical results produced by our implementation of the FP method compare to simulations done using the SPARTA DSMC code[18] as well as to experimental data produced at DLR Goettingen.[4,15] We show that the FP method leads to very similar results as DSMC for N_2 flow impingement on a flat plate while providing a 4 fold speedup when using the same grid and temporal resolution. We compare results for surface pressure, shear stress as well as heat flux. The FP simulations were performed using the cubic formulation[5] extended with the master equation anstaz to model internal degrees of freedom.[11]

DOI: 10.13009/EUCASS2023-385

2. Method

2.1 Cubic Fokker-Planck

As the cubic formulation of the FP method was covered in detail in literature[5,7,8] we will be giving only a briefly summary here.

The well-known Boltzmann equation describes the evolution of a scalar distribution function f due to intermolecular collisions in rarefied flows:

$$\frac{\mathrm{D}f}{\mathrm{D}t} = S_{\mathrm{Boltz}} \,, \tag{1}$$

where t is time and S_{Boltz} is the Boltzmann collision integral. A recently introduced approach[12] to make the integro-differential Eq. (1) more manageable is to approximate S_{Boltz} by a Fokker-Planck collision operator S_{FP}:

$$S_{\mathrm{Boltz}} \approx S_{\mathrm{FP}} = -\frac{\partial}{\partial V_i}(A_i f) + \frac{\partial^2}{\partial V_j \partial V_j}(D^2 f) \,, \tag{2}$$

where the drift coefficient A_i and the diffusion coefficient D of Eq. (2) are model parameters chosen in such a way that production terms calculated using the Boltzmann collision operator are reproduced in the continuum limit. According to Itô's lemma, Eqn. (2) can be written as a stochastic differential equation

$$\frac{\mathrm{d}\mathbf{X}}{\mathrm{d}t} = \mathbf{V}, \tag{3}$$

$$\frac{\mathrm{d}\mathbf{V}}{\mathrm{d}t} = \mathbf{A} + D\frac{\mathrm{d}\mathbf{W}}{\mathrm{d}t} + \mathbf{F} \,, \tag{4}$$

with $\mathbf{X}$ denoting particle position, $\mathbf{V}$ the particle velocity and $\mathrm{d}\mathbf{W}$ the Wiener process with zero expectation. Thus, the resulting Fokker-Planck equation can be solved through stochastic motion which in turn can be modeled using a particle method. For a single species gas using the cubic model[5] the drift A_i and the diffusion coefficient D are chosen as

$$A_i = -\frac{1}{\tau}C_i + \xi_{ij}C_j + \gamma_i\left(C_jC_j - \frac{3k_\mathrm{B}T}{m}\right) + \Lambda\left(C_iC_jC_j - \frac{2q_i}{\varrho}\right), \tag{5}$$

$$D = \sqrt{\frac{2k_\mathrm{B}T}{\tau m}} \,. \tag{6}$$

where τ is a relaxation time, γ and ξ are the coefficient matrices, k_B is the Boltzmann constant, T the temperature, m is mass, $\mathbf{q}$ the heat flux vector and ϱ the (mass) density. The parameter Λ is chosen to assure stability of the model. Eqn. (4) can be integrated leading to

$$V^{n+1} = \frac{1}{\alpha}\left[C_i^n \exp\left(-\frac{\Delta t}{\tau}\right) + \left(1 - \exp\left(-\frac{\Delta t}{\tau}\right)\right)\tau N_i^n + \psi_i\sqrt{\frac{D^2}{2}\tau\left(1 - \exp\left(-2\frac{\Delta t}{\tau}\right)\right)}\right] + V_i^n - C_i^n \,, \tag{7}$$

where $\mathbf{C}$ denotes the thermal particle velocity. The nonlinear term $\mathbf{N}$ can be expressed as

$$N_i^n = \xi_{ij}C_j^n + \gamma_i\left(C_j^nC_j^n - \frac{3k_\mathrm{B}T}{m}\right) + \Lambda\left(C_i^nC_j^nC_j^n - \frac{2q_i}{\varrho}\right) \,. \tag{8}$$

Here the factor α is a parameter used to scale particle velocities to ensure energy conservation for arbitrary time steps. To be compatible with DSMC a simple integration scheme for particle positions is chosen as

$$\mathbf{X}^{n+1} = \mathbf{X}^n + \mathbf{V}^n\Delta t \,. \tag{9}$$

2.2 Master Equation Anastz

Since its inception several modifications have been introduced to model internal degrees of freedom using the FP method.[6,16,17] Our implementation uses the master equation ansatz.[11] The basic premise behind the model is the fact that the Boltzmann collision operator can be split into an elastic $S^{\mathrm{el}}_{\mathrm{Boltz}}$ and an inelastic part $S^{\mathrm{inel}}_{\mathrm{Boltz}}$:

$$S_{\mathrm{Boltz}} = S^{\mathrm{el}}_{\mathrm{Boltz}} + S^{\mathrm{inel}}_{\mathrm{Boltz}} \,. \tag{10}$$

DOI: 10.13009/EUCASS2023-385

The goal is to approximate both parts in such a way as to stay consistent with the Fokker-Planck formulation. The elastic operator is formulated as before, but only a fraction of the particles undergo the elastic collisions. The inelastic part may again be split into two parts:

$$S_{\text{Boltz}}^{\text{inel}} = S_{\text{v}} + S_{\text{e}} \ , \tag{11}$$

where S_{v} describes the change of the number of particles in a phase space element due to a change of particle velocities and S_{e} refers to the change in the number of particles in a phase space element due to a change of internal energies as a result of inelastic collisions. The first part can be modeled via the Fokker-Planck ansatz described above, where the diffusion coefficient is modified to account for energy transfer between translational and internal degrees of freedom. The second part is modeled using the master equation ansatz as

$$S_{\text{e}} = \sum_j \left(R_{j,m} f_j - R_{n,j} f_n \right) \ . \tag{12}$$

Here $R_{q,k}$ are the rate coefficients modeling the transition rates between the internal energy states q and k. When combined with the original FP equation the new FP-Master Equation can be written as

$$\frac{\mathrm{D}f_n}{\mathrm{D}t} = \tilde{S}(f_n) + \sum_j \left(R_{j,m} f_j - R_{n,j} f_n \right) \ . \tag{13}$$

where $\tilde{S}(f_n)$ is the FP operator with the modified diffusion coefficient. Assuming that the evolution of translational velocities and internal energies can be modelled as independent stochastic processes, it can be written:

$$f_n(\mathbf{r}, \mathbf{v}, t) = f(\mathbf{r}, \mathbf{v}, t)\ g_n(\mathbf{r}, t) \ . \tag{14}$$

Eqn. (13) can now be separated into a set of equations

$$\frac{\mathrm{d}f}{\mathrm{d}t} = \frac{\mathrm{d}f}{\mathrm{d}t} + \frac{\mathrm{d}f}{\mathrm{d}x_i} v_i = \tilde{S}(f_n) \tag{15}$$

$$\frac{\mathrm{d}g_n}{\mathrm{d}t} = \frac{\mathrm{d}g_n}{\mathrm{d}t} + \frac{\mathrm{d}g_n}{\mathrm{d}x_i} v_i = \sum_j \left(R_{j,m} f_j - R_{n,j} f_n \right) \ , \tag{16}$$

which are solved independently each time step.

The transfer of energy between the internal degrees of freedom is implicitly modeled in the rate coefficients. The coefficients can be divided into two groups: discrete and continuous. Hepp *et al.*[11] proposed two types of coefficients: *Landau-Teller relaxation* based coefficients using the continuous (CLT) and discrete (DLT) model for internal energies and *Larsen-Borgnakke relaxation* based coefficient using a discrete energy model (DLB). For the simulations presented in this paper we used the CLT to model the rotational and DLT to model vibrational energy relaxation respectively.

3. Numerical Analysis

3.1 Experimental Setup

In our analysis we use data from experiments which were performed at the German Test and Research Institute for Aviation and Space Flight (DFVLR), now named German Aerospace Center (DLR). Two experiments taken from two different test campaigns were used as a comparison. Both campaigns were extensive investigations of effects caused by impingement of a molecular nitrogen plume on a flat plate under the considerations of various angles between the plume and the plate. The first one, performed by Doering,[4] investigated the heat flux on the plate. The second, performed by Legge,[15] investigated pressure and shear stress. The experimental setup can be seen in Figure 1 were p_0 and T_0 are stagnation values inside the plenum. To obtain the data for pressure and shear stress a pressure balance was used that measured the force on a floating element. For the heat flux the rate of change of surface temperature was measured using thermocouples. The measurements were performed on the surface along a line coplanar with the plume axis. In the experiments referenced in this paper the same orifice was used for the plume generation. Through it unheated flow ($T_0 = 300\,\text{K}$) expands from a stagnation pressure of $p_0 = 1000\,\text{Pa}$. The orifice itself is circular in cross section, has a radius of $r^* = 1\,\text{mm}$, and the flow is assumed to be sonic at the exit.

The experimental data was used in the past to validate DSMC simulations.[13] To provide comparison the same subset of experiments was chosen for our analysis. The data was selected to provide reasonable conditions for a DSMC as well as FP simulation. The relevant physical data is summed up in Table 1. Here L is the distance from the orifice to the flat plate. The main differences in the values presented between the two experiments is the background pressure which was higher in the heat flux case.

DOI: 10.13009/EUCASS2023-385

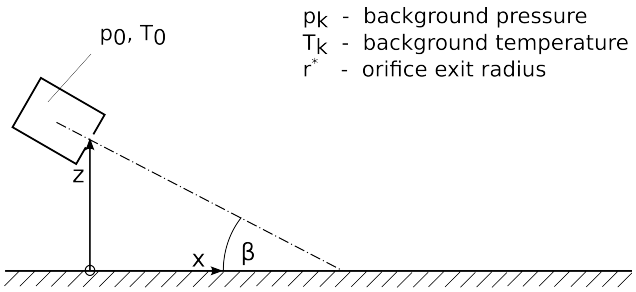

Figure 1: Experimental setup.

Table 1: Experimental parameters.

	p_0 / Pa	p_k / p_0	r^* / mm	L / r^*	β
Legge[15]	1000	4.5×10^{-5}	1	40	90°
Doering[4]	1000	9×10^{-5}	1	40	90°

3.2 Simulation Setup

The numerical results were obtained in 3D simulations with the domain being a 90° section of the plume with the origin being in the center of the orifice as seen in Figure 2. The symmetry condition was realized using two specular reflecting

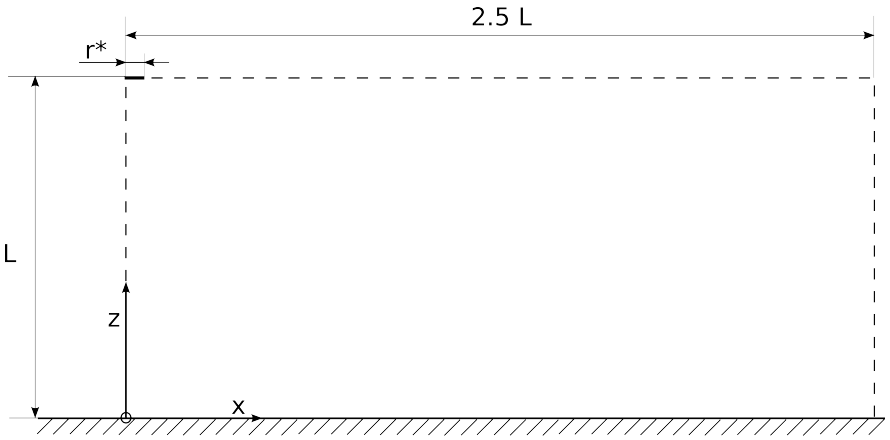

Figure 2: Side view of the simulation domain.

walls as seen in Figure 3. The domain size in x and y direction was chosen to be $2.5 \times L$ for all simulations. For the plate diffusive scattering was assumed with a wall temperature of $T_w = 300$ K and an accommodation coefficient of 1. The inflow conditions were calculated using isentropic expansion and are summarized together with other boundary conditions in Table 2. For the simulations of pressure and shear stress a particle weight of $w = 1 \times 10^8$ was used while

Table 2: Simulation parameters.

	n / m^{-3}	T / K	u / m s^{-1}
Inflow	1.531×10^{23}	250	322.366
Background, Legge[15]	1.086×10^{19}	300	0
Background, Doering[4]	2.173×10^{19}	300	0

for the simulation of the heat flux a weight $w = 2 \times 10^8$ was chosen due to higher background pressure. A time step of $\Delta t = 1 \times 10^{-6}$ s was employed in all cases. To reach steady state a pre-run of 700 steps was performed for each simulation. The displayed results were obtained by time averaging over 2000 steps. The simulations were run on a single node of the CARO HPC cluster. The specifications of the node are summarized in Table 3.

DOI: 10.13009/EUCASS2023-385

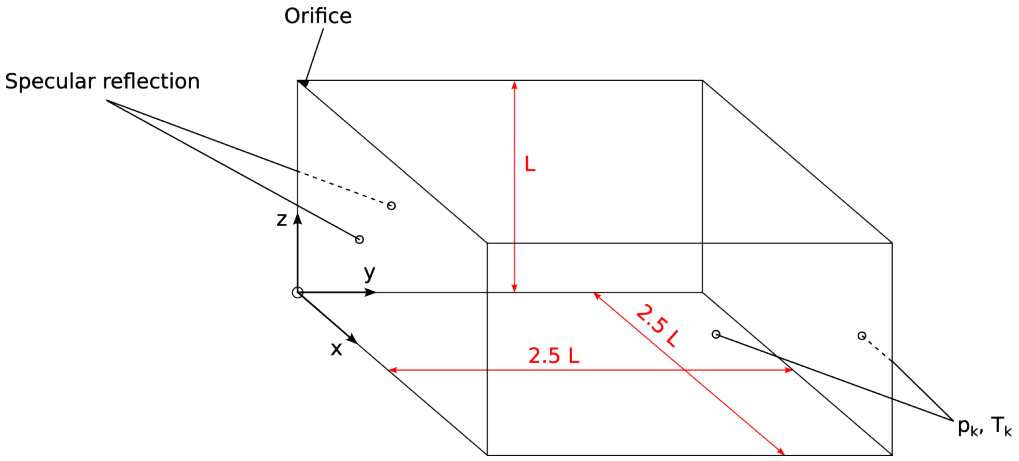

Figure 3: 3D view of the simulation domain.

Table 3: Specifications of a node at the CARO HPC cluster.

CPU	2x AMD EPYC 7702 (64 cores; 2.0 GHz)
RAM	256 GB DDR4 (3200 MHz)
Hard Drive	4 x NVMe SSD

3.3 Numerical Results and Discussion

A very good agreement is seen between the flow fields calculated using DSMC and FP. The results for the magnitude of the velocity component perpendicular to the flat plate for the Legge[15] test case are visualized in Figure 4. This

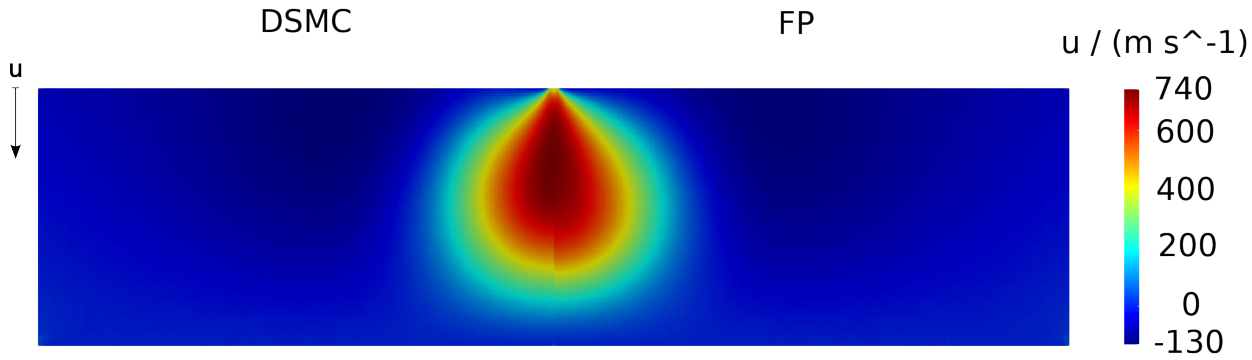

Figure 4: Molecular nitrogen flow field. The colors present the magnitude of the velocity component perpendicular to the flat plate.

agreement is also seen quantitatively in the values calculated on the surface of the flat plate. The results for surface pressure p and shear stress τ are presented in dimensionless quantities as seen in Eqn. (17) and Eqn. (18).

$$\tilde{p} = \frac{p}{p_0}\left(\frac{L}{r*}\right)^2 \tag{17}$$

$$\tilde{\tau} = \frac{\tau}{p_0}\left(\frac{L}{r*}\right)^2 \tag{18}$$

DOI: 10.13009/EUCASS2023-385

Results for the normalized pressure are displayed in Figure 5. Very good agreement can be seen between the

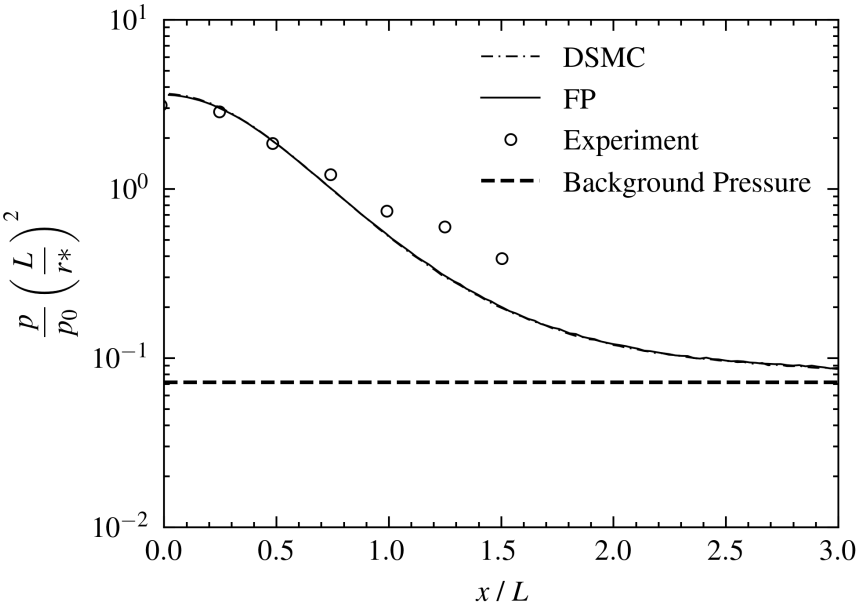

Figure 5: Surface pressure.

DSMC and FP solutions. The relative error between the two is visualized in Figure 6(a). Both are in good agreement to the experimental results close to the plume center line but deviate as the distance becomes larger. This can be seen more clearly in relative error between the solution produced by the FP method compared to the the experimental data which is displayed in Figure 6(b). The same behavior was reported by Kannenberg and Boyd.[13] The deviation can most likely be explained by difficulties in measuring pressure in more rarefied areas. Additionally Kannenberg and Boyd speculate that the background pressure during the experiment was higher than reported since the values do not show a convergence towards the reported background pressure as seen in the numerical results.

Figure 7 shows comparison of the results for the normalized shear stress. Again very good agreement can be observed between the FP and DSMC results as seen in Figure 8(a). The relation to the experimental data is also very similar to that observed by literature. The relative error of FP results to experimental data is shown in Figure 8(b).

The comparison of simulation and experimental results for the heat flux is shown in Figure 9. The agreement between the FP and DSMC results is again very good as seen in the relative error between the two in Figure 10(a). Both show high levels of fluctuation away from the beam centerline which in part is due to the the decreasing number of particles available for sampling in the more rarefied areas. This effect is magnified by the fact that heat flux is a higher order moment compared to pressure and shear stress thus requiring a bigger sample size to provide low noise results. The high deviation in comparison to the experimental data as illustrated in Figure 10(b) was also observed by Kannenberg and Boyd.[13] This can in part be explained by the difficulties in capturing heat flux both experimentally as well as numerically due to the high order of the moment. It is important to note that both the FP as well as the DSMC simulations produce very similar results which shows that the deviation to experiments does not necessarily come from the choice of the collision model but rather from the treatment of the gas surface interactions. Our simulations as well as DSMC simulations from literature model these interactions via diffusive scattering with an accommodation factor of 1. The investigation of the impact of the choice of the gas-surface model lies outside of the scope of this paper and is left for future work.

During the investigation the total computational times between of the FP and DSMC simulations were recorded. The results can be seen in Table 4. The times were taking using the same parameters for both the DSMC and FP

Table 4: Comparison of computational time between FP and DSMC.

	DSMC	**FP**	**Speedup**
Experiment Legge	24 909.1 s	5422.3 s	4.6
Experiment Doering	12 747.0 s	3280.2 s	3.9

simulation in each case: number of particles, spatial and temporal resolutions as well as number of time steps executed.

DOI: 10.13009/EUCASS2023-385

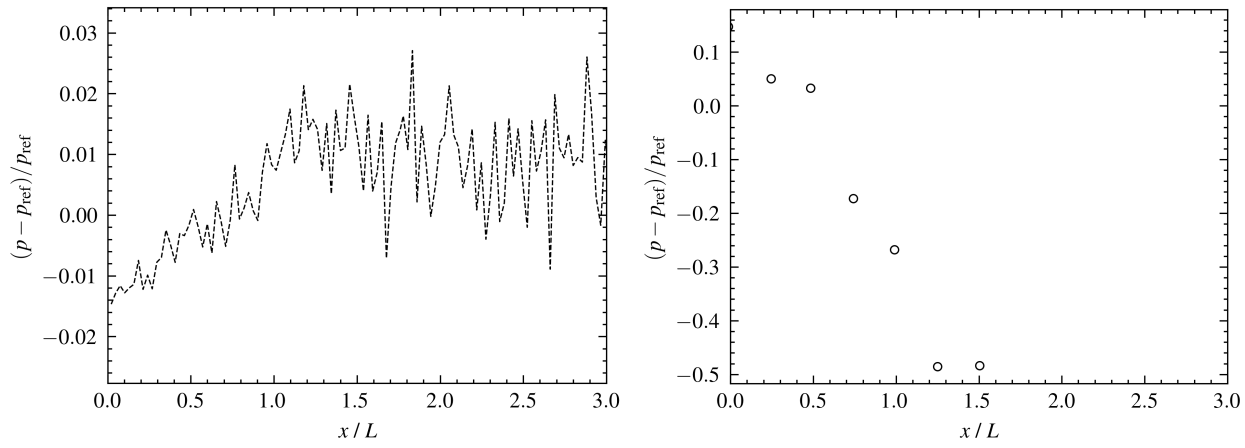

(a) FP compared to DSMC.

(b) FP compared to experimental data.

Figure 6: Relative error in surface pressure.

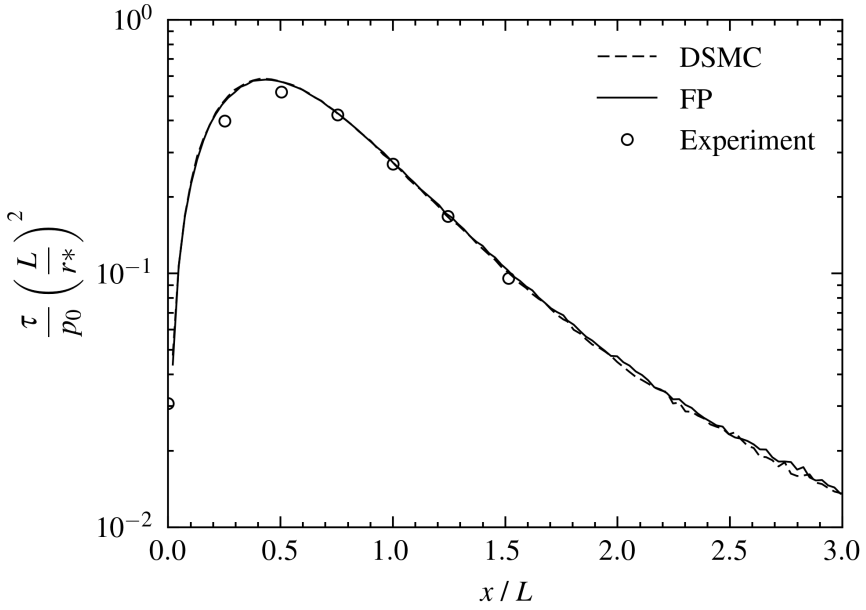

Figure 7: Surface shear stress.

It is clear that for both setups a significant speed up can be achieved (around 4 in both cases). The slightly lower speedup in the case of the heat flux experiment can be explained the the higher particle weight chosen due to the higher background pressure for the simulation as it reduces the number of collisions calculated for the DSMC solution and thus its computational cost.

4. Conclusion and Outlook

Simulations of plume impingement on a flat plate using molecular nitrogen were performed by employing the FP and DSMC methods. The simulations are based on two experimental campaigns performed at DLR Goettingen. One measuring surface pressure and shear stress and the other surface heat flux. In both cases very good agreement between the numerical results produces by our FP and DSMC simulations is observed. The same can be said when comparing our results to DSMC simulations found in literature which are based on the same experiments. For the selected cases a considerable speed up of around 4 fold for the FP simulations compared to simulations using DSMC is found when using the same spatial and temporal resolution. Comparisons to experimental data is also very favorable in the cases of pressure and shear stress calculated on the flat plate. The results for the surface heat flux show a high deviation to

DOI: 10.13009/EUCASS2023-385

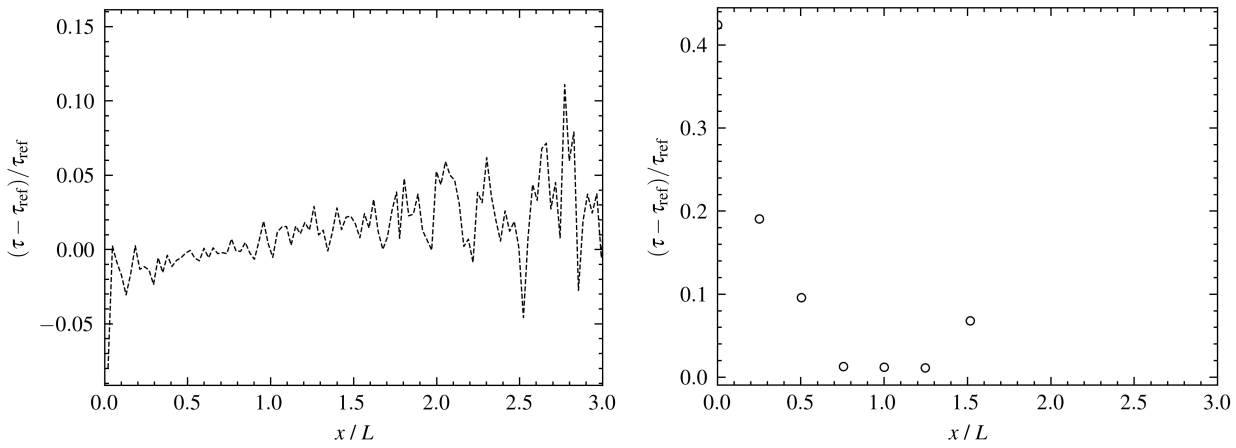

(a) FP compared to DSMC.

(b) FP compared to experimental data.

Figure 8: Relative error in surface shear stress.

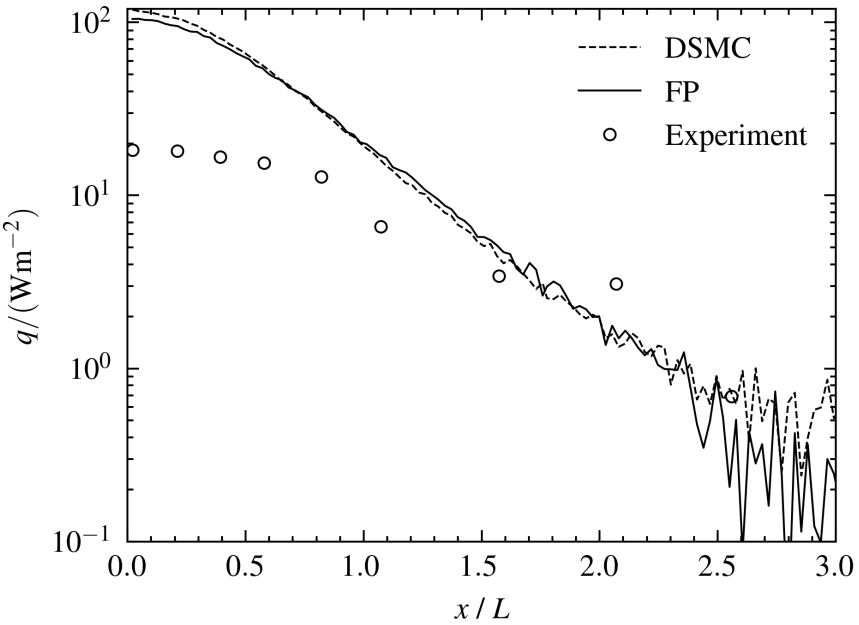

Figure 9: Surface heat flux.

experimental data. However, it is important to note that both FP and DSMC methods produce very similar results when using the same assumptions. This shows that in certain cases FP can be a viable alternative to DSMC for generating high fidelity results when simulating rarefied flows while calling for a significantly lower computational cost.

It is open for future work to investigate whether the boundaries of applicability can be extended further for the FP method. This would allow for faster and more effective cycles in space craft design thus reducing risk and cost for the industry.

5. Acknowledgments

The authors would like to thank Alexander von Humboldt Foundation-supported research fellow Dr. Georgii Oblapenko for helpful discussions and his insights provided on the topic of DSMC and plume simulations.

DOI: 10.13009/EUCASS2023-385

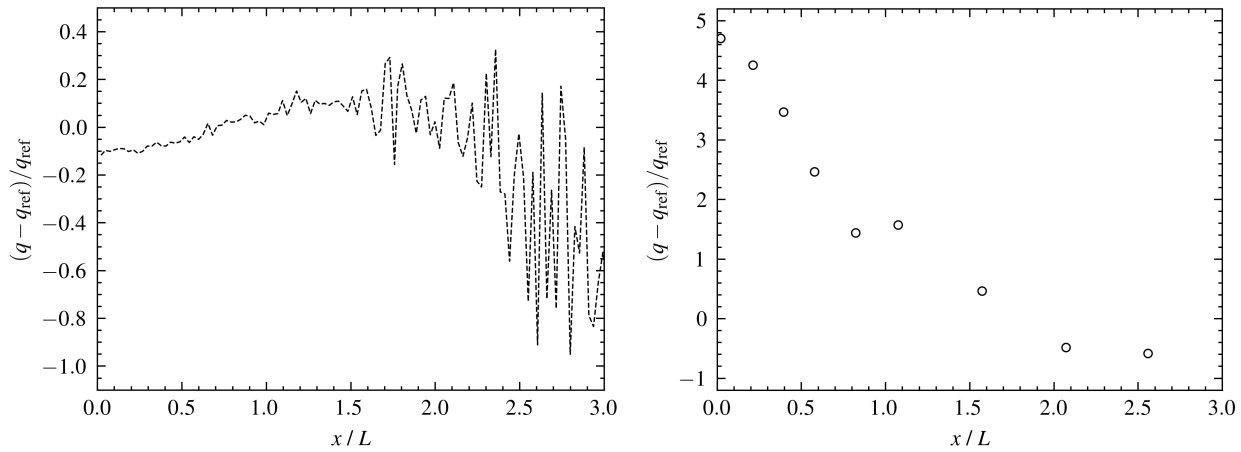

(a) FP compared to DSMC.

(b) FP compared to experimental data.

Figure 10: Relative error in surface heat flux.

References

[1] G. A. Bird. *Molecular Gas Dynamics and the direct Simulation of Gas Flows*. Oxford University Press, New York, 1994.

[2] S. V. Bogomolov. On Fokker-Planck model for the Boltzmann collision integral at the moderate Knudsen numbers. *Mathematical Models and Computer Simulations*, 1(6):739–744, December 2009.

[3] George Dettleff. Plume flow and plume impingement in space technology. *Progress in Aerospace Sciences*, 28(1):1–71, January 1991.

[4] Stephan Döring. Experimental plume impingement heat transfer on inclined flat plates. 1990.

[5] M. H. Gorji, M. Torrilhon, and P. Jenny. Fokker-Planck model for computational studies of monatomic rarefied gas flows. *Journal of Fluid Mechanics*, 680:574–601, August 2011.

[6] M. Hossein Gorji and Patrick Jenny. A Fokker-Planck based kinetic model for diatomic rarefied gas flows. *Physics of Fluids*, 25(6):062002, June 2013.

[7] M. Hossein Gorji and Patrick Jenny. An efficient particle Fokker-Planck algorithm for rarefied gas flows. *Journal of Computational Physics*, 262:325–343, April 2014.

[8] M. Hossein Gorji and Patrick Jenny. Fokker-Planck-DSMC algorithm for simulations of rarefied gas flows. *Journal of Computational Physics*, 287:110–129, April 2015.

[9] M. Hossein Gorji and Manuel Torrilhon. Entropic Fokker-Planck kinetic model. *Journal of Computational Physics*, 430:110034, April 2021.

[10] Bijiao He, Jianhua Zhang, and Guobiao Cai. Research on vacuum plume and its effects. *Chinese Journal of Aeronautics*, 26(1):27–36, February 2013.

[11] Christian Hepp, Martin Grabe, and Klaus Hannemann. Master equation approach for modeling diatomic gas flows with a kinetic Fokker-Planck algorithm. *Journal of Computational Physics*, 418:109638, October 2020.

[12] Patrick Jenny, Manuel Torrilhon, and Stefan Heinz. A solution algorithm for the fluid dynamic equations based on a stochastic model for molecular motion. *Journal of Computational Physics*, 229(4):1077–1098, February 2010.

[13] Keith C. Kannenberg and Iain D. Boyd. Three-Dimensional Monte Carlo Simulations of Plume Impingement. *Journal of Thermophysics and Heat Transfer*, 13(2):226–235, April 1999.

DOI: 10.13009/EUCASS2023-385

[14] Kyun Ho Lee. Satellite design verification study based on thruster plume flow impingement effects using parallel DSMC method. *Computers & Fluids*, 173:88–92, September 2018.

[15] H. Legge. *Plume impingement forces on inclined flat plates*. January 1991. Conference Name: Rarefied Gas Dynamics Pages: 955-962 ADS Bibcode: 1991rgd..proc..955L.

[16] J. Mathiaud and L. Mieussens. A Fokker-Planck Model of the Boltzmann Equation with Correct Prandtl Number for Polyatomic Gases. *Journal of Statistical Physics*, 168(5):1031–1055, September 2017.

[17] J. Mathiaud and L. Mieussens. BGK and Fokker-Planck Models of the Boltzmann Equation for Gases with Discrete Levels of Vibrational Energy. *Journal of Statistical Physics*, 178(5):1076–1095, March 2020.

[18] S. J. Plimpton, S. G. Moore, A. Borner, A. K. Stagg, T. P. Koehler, J. R. Torczynski, and M. A. Gallis. Direct simulation Monte Carlo on petaflop supercomputers and beyond. *Physics of Fluids*, 31(8):086101, August 2019.

[19] Jun Zhang, Benzi John, Marcel Pfeiffer, Fei Fei, and Dongsheng Wen. Particle-based hybrid and multiscale methods for nonequilibrium gas flows. *Advances in Aerodynamics*, 1(1):12, December 2019.